VANLANDUIT, S., SORGENTE, M., ZADEH, A.R., GÜEMES, A. and FAISAL, N. 2021. Strain monitoring. In *Sause, M.G.R. and Jasiūnienė, E. (eds.) Structural health monitoring damage detection systems for aerospace.* Springer aerospace technology. Cham: Springer [online], chapter 8, pages 219-241. Available from: https://doi.org/10.1007/978-3-030-72192-3_8

Strain monitoring.

VANLANDUIT, S., SORGENTE, M., ZADEH, A.R., GÜEMES, A. and FAISAL, N.

2021

Chapter 8
Strain Monitoring

Steve Vanlanduit, Mario Sorgente, Aydin R. Zadeh, Alfredo Güemes, and Nadimul Faisal

Abstract This chapter provides an overview of the use of strain sensors for structural health monitoring. Compared to acceleration-based sensors, strain sensors can measure the deformation of a structure at very low frequencies (up to DC) and enable the measurement of ultrasonic responses. Many existing SHM methods make use of strain measurement data. Furthermore, strain sensors can be easily integrated in (aircraft) structures. This chapter discusses the working principle of traditional strain gauges (Sect. 8.1) and different types of optical fiber sensors (Sect. 8.2). The installation requirements of strain sensors and the required hardware for reading out sensors are provided. We will also give an overview of the advantages and the limitations of commonly used strain sensors. Finally, we will present an overview of the applications of strain sensors for structural health monitoring in the aeronautics field.

8.1 Strain Gauges

A strain gauge (or gage) is a sensing device used to determine the directions and magnitudes of principal surface strains (ASTM E1561-93 2014) and residual stresses (ASTM E837-13a 2013) in conjuction with established algorithms. Once the surface on which the strain gauge is assembled is deformed, the strain gauge causes a change in length leading to a change in electrical resistance. The change in electrical

S. Vanlanduit (✉)
University of Antwerp, Antwerp, Belgium
e-mail: steve.vanlanduit@uantwerpen.be

M. Sorgente · A. R. Zadeh
Optics 11, Amsterdam, The Netherlands

A. Güemes
Technical University of Madrid, Madrid, Spain

N. Faisal
Robert Gordon University, Aberdeen, UK

M. G. R. Sause, E. Jasiūnienė (eds.), *Structural Health Monitoring Damage Detection Systems for Aerospace*, Springer Aerospace Technology,
https://doi.org/10.1007/978-3-030-72192-3_8

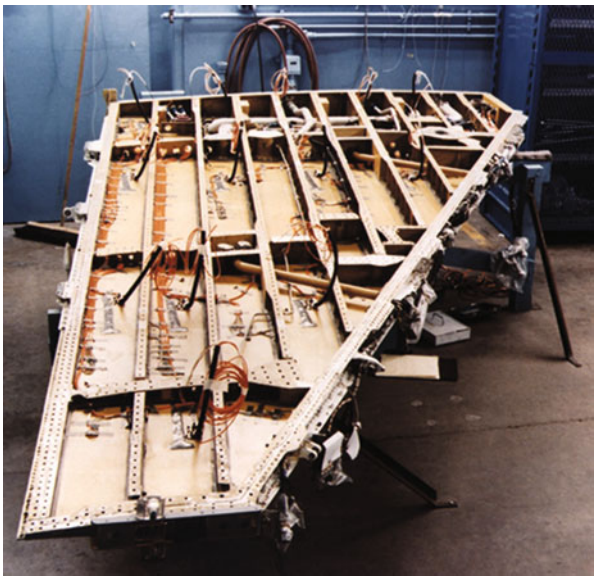

Fig. 8.1 Strain gauge installation on metallic aircraft structures (installed in the interior of the AFTI/F-16 wing at NASA DFRC) (Anon. 1984)

resistance is measured using an electrical circuit (i.e. Wheatstone bridge), which is then related to strain by the quantity known as the gauge factor. The stress is force per unit of surface (i.e. pressure) that is acting on an infinitesimal area. The stress is a derived quantity that under some assumptions (e.g. single axis stress state and strain measured in the transverse direction) can be calculated from the strain (if the Young's modulus is known). In general the measured strain depends on the mechanical load as well as the thermal loading. When establishing the stress-strain relationship both contributions should be balanced. Furthermore in case of permanent or plastic deformation of a material setting up the relation between the measured strain and the stresses (including residual stress) is much more difficult (Faisal et al. 2019).

Figure 8.1 shows the strain gauge installation inside an aircraft wing structure (Anon. 1984). To prepare any surface or structure of interest to assemble the strain gauge, grit-based sandpaper is typically used to largely remove any debris or rust to increase the contact surface area of the surface face with the bonding agent sandwiched with the strain gauge (Anon. 1984). Following which, alcohol-based solutions are used to decontaminate the material surface. The adhesive glue for the strain gauge assembly is applied and let to cure in ambient conditions for a high bond strength. The adhesive type may affect the bonding quality with the test surface, and control measures may be necessary for verifying the installation features.

Even in the case of uni-axial loading, bi-directional strains often need to be measured. In the case of a purely compressive load of a beam for instance, tensile strain would be induced at 90° to the compressional strain direction. This is of interest in a number of aircraft structures; therefore, bi-element strain gauges are typically used during testing. Strain relief must be considered during testing. Typically, a thin plastic layer is glued on top of the components to relieve some of the

stress exerted. Excess plastic is then removed after the glue sets. A commercially available programmable automation controller (e.g. National Instruments, Vishay Precision Group) can be used to receive the signals created by strain gauges. The instrumentation includes strain indicators, signal conditioning amplifiers, and software for data recording. The strain gauge would normally come with a shorter lead cable length (e.g. recommended length of 1.5–2.5 m, (IPC/JEDEC 2005). Quarter-bridge strain gauges in a 'three-wire connection' are preferred over those in a 'two-wire connection.' The increase in the lead wire length increases the possibility of errors due to temperature variations, lead desensitization, and lead-wire resistance changes (ASTM E1561-93 2014). A slight change in the temperature can generate a measurement error of several microstrain. For the extension of strain gauge cables, a careful consideration is needed when extending to long lengths because the overall resistance of the strain gauge assembly will change (Takeuchi 2012).

For aircraft SHM, the complex geometry of the structures (specimen) leads to a complex strain analysis. Usually assumptions of a much simpler strain distribution are made in practice (e.g. by ignoring the strain in the thickness direction of a thin beam). Due to a combination of the high sensitivity of the strain gauge measurement equipment, outdoor environment, and necessity for extremely long data cables, the raw data could feature a high noise level. To minimise the effects of such noise and allow trends to be more clearly identified, the signals (for each strain gauge) can be smoothed by averaging over a window of data points using a computational code, thereby removing localised spikes that could potentially be seen in the raw data. Despite data smoothing, there can still be a fluctuation due to the low signal-to-noise ratio, which makes it difficult to identify significant events within the test from the strain gauge data alone.

8.2 Optical Fiber Sensors

8.2.1 Introduction

In a fiber optic sensor, light guided through the fiber core is affected by the measurand. Optical fiber sensors (OFS) are most frequently used to measure strain, temperature, or pressure, but they can also be used as chemical sensors, vibroacoustic detectors and refractometers for cure monitoring (Lee 2003). One of the main advantages of the optical fiber sensor is its thinness. It usually has a diameter of 125μm, but OFS with a diameter of up to 12μm have also been reported (Malik et al. 2016). This makes it easy to integrate them in materials like composite materials. In the last few decades, the OFS have been successfully used for damage detection in composite materials (Kinet et al. 2014).

In composite materials, OFS are sandwiched between two composite layers (Dawood et al. 2007). This process has been successfully applied to aircraft components at Airbus (Giraldo et al. 2017).

In metals, OFS are also being integrated in components (Saheb and Mekid 2015; He et al. 2019). In this case, fiber is inserted in a groove closed by melting subsequent powder layers on top of the fibers (Havermann et al. 2015). Metal melting is usually performed by laser cladding or high-power ultrasound (He et al. 2019). A metal (Grandal et al. 2018) or carbon (Nedjalkov et al. 2018) coating is applied to protect the fibers from high temperatures during the integration process.

In other applications, the OFS is not integrated in the material under test, but the sensors are applied at the surface of the part. This can be done by using a prepreg sample with an integrated optical fiber, of which the so-called fiber optic ribbon tape (FORT) is an example (Loutas et al. 2015). For aerospace applications, a specialty aerospace-grade coated fiber Bragg gratings (FBG) sensor with an adapted bonding procedure was developed (Goossens et al. 2019). Goossens et al. tested their sensor in in-flight conditions with realistic humidity, temperature, and pressure cycles, as well as hydraulic fluid and fatigue loading.

Optical fiber sensors can be used in harsh environments (Mihailov 2012). They are immune to electromagnetic interference (Druet et al. 2018) and can be used at very high temperatures. Silica glass allows the detection of strains in environments up to 1000 °C (Yu and Okabe 2017). Radiation-hardened sensors have been developed for space applications (Girard et al. 2018).

Another important advantage of OFS is the fact that they can be multiplexed. Several sensors can be inscribed in one optical fiber, and these sensors can be read out using one single interrogator. The interrogator is the hardware needed to acquire the measurand from the reflected or transmitted light that goes through the fiber. Time domain multiplexing has been used to realise up to 1000 ultra-weak FBG for distributed temperature sensing (Wang et al. 2012) and 100s of strain sensors (Dai et al. 2009; Cranch and Nash 2001). In addition to the point sensors, also distributed fiber optics sensors based on different principles are available: Rayleigh (Froggatt et al. 1998) and Brillouin scattering (Garus et al. 1996).

8.2.2 Types of Optical Fiber Sensors

Sensors vitally affect our life in multiple fields, such as IoT, structural health monitoring, smart structures, and digital twins. The necessity of tracking the material behavior has assumed a great, and not trivial importance in reducing maintenance costs and promoting prevention over replacement. In addition, the harsher the environment, the more challenging the measurement. The advantages of optical sensors come into play because of the fact that they are

- completely passive,
- lightweight,
- survive at critical temperature, dust, and ATEX (ATmosphere EXplosible) environment,
- immune to electromagnetic interference,

- not required to have pre-amplification, and
- capable of being interrogated from hundreds of meters of distance.

These features open up scenarios for more accurate, precise, and repeatable measurements (Pinet 2009). This study discusses some of the most common optical sensing techniques based on the interferometry principle.

8.2.3 *Interferometry*

Interferometry is a technique based on the wave interference phenomenon. In classic physics, this comes into play when two waves superimpose to generate a resultant wave of a greater (constructive interference) or lower amplitude (destructive interference). The former occurs when the phase difference of the two waves is an even multiple of π (180°), whereas the latter happens when the difference is an odd multiple of π. The phase differences with values between these two extremes will result in displacement magnitudes that range between the minimum and maximum values. Two conditions must be met to set up an interference pattern that is stable and clear (Hariharan 2007):

1. *Coherent light sources must be used*, meaning they emit waves with a constant phase difference.
2. The waves should be of a single wavelength, that is, monochromatic.

Several types of interferometers are available and have a wide-spread use in optical sensing applications. Interferometry based optical sensors can be easily scaled up to long ranges, used in satellite imaging of surface deformation, and scaled down to cell stiffness measurement in biological matters. Furthermore, the sensitivity of these sensors can be tuned by adjusting the interferometry arm lengths of the sensor. For these reasons, the interferometry principle has become a basis for numerous sensor designs in both academia and in the industry.

In this article, three of the most common interferometer types will be discussed, namely Mach–Zehnder, Michelson, and Fabry–Pérot.

8.2.4 *Mach–Zehnder*

In optics, the Mach–Zehnder interferometer is an optical device capable of determining the relative phase shift variation between the superposition of two collimated beams. Figure 8.2 shows the working principle. A light beam is shined on a beam splitter that divides it into two parts. The traveling different paths will be reflected on the mirrors and recombined on a second beam splitter, then directed on the photodetectors to be acquired (Zetie et al. 2000).

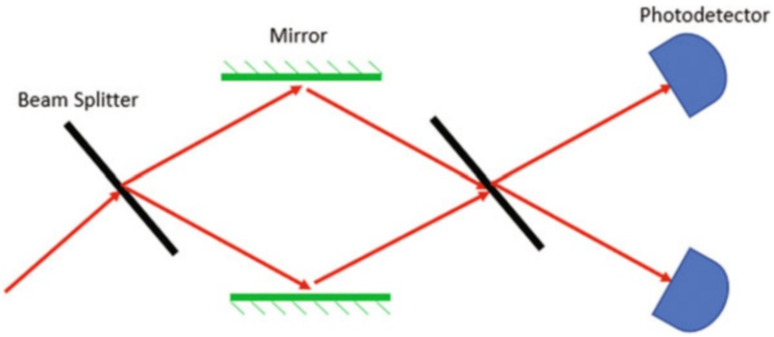

Fig. 8.2 Schematic of a Mach–Zehnder interferometer

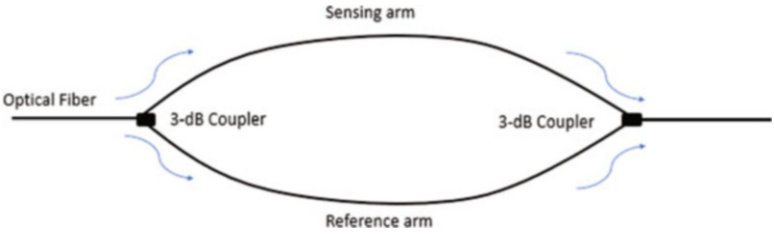

Fig. 8.3 Mach–Zehnder interferometer: integrated configuration

Mach–Zehnder interferometers (MZIs) have been implemented as optical devices in multiple sensing applications because of their flexible configurations (Bahrampour 2012). Their optical fiber integrated version is based on the same working principle using a different optical element (Fig. 8.3). The incident beam is split into two arms and recombined into one using two fiber couplers. For sensing applications, the reference arm is ideally isolated from the external variations, and only the sensitive arm experiences changes. The information is kept in the optical path difference between the two arms, which as discussed in the previous section, can be detected by calculating the interference signal variation.

The physical quantities that externally affect the sensing arm change its length, thereby generating a phase difference between the beams traveling the reference and the sensing arms. The optical phase delay $\varnothing$ can be expressed as follows:

$$\varnothing = nkL \tag{8.1}$$

where, n is the refractive index, and L is the fiber length. The product nL represents the optical path length, and k is the wavenumber (Zahid et al. 2019).

8.2.5 *Michelson Interferometer*

Similar to the Mach–Zehnder interferometer, the Michelson interferometer (MI) compares two beams reflected from two mirrors on two configuration branches. An MI is considered as half of an MZI, where the main difference is the presence of two reflectors.

In the Michelson interferometer in Fig. 8.4, light is shined from a coherent light source on a beam splitter that splits the light into two different optical paths. The reflected and transmitted waves are recombined to let them interfere on a photodetector. The beam splitter placed at an angle of 45° with respect to the incoming laser beam distributes the light equally to both mirrors. The following relationship is valid on the photodetector:

$$2D = n\lambda \tag{8.2}$$

where, D distance of the movable; n number of interferometric fringes; λ beam wavelength.

Figure 8.5 depicts a fiber-based model of an MI. Light travels through the sensitive and reference arm, thereby being distributed and recombined by an optical coupler. The external physical quantity affects the sensitive arm that will modify its lengths accordingly. The output in terms of the phase change is processed at the port where the photodetector is connected (Zahid et al. 2019).

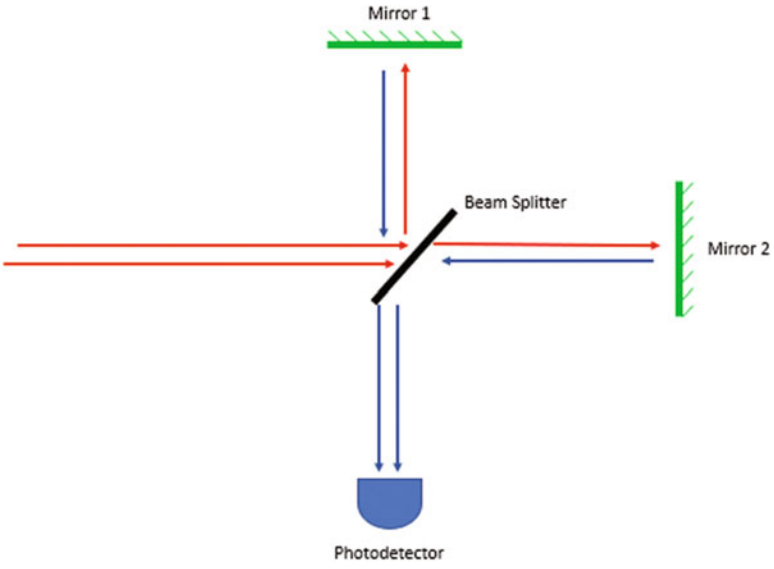

Fig. 8.4 Configuration of a Michelson interferometer

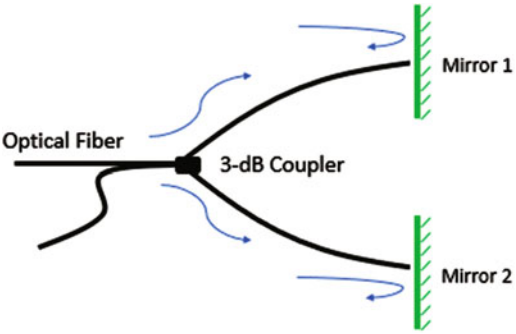

Fig. 8.5 Michelson interferometer: integrated configuration

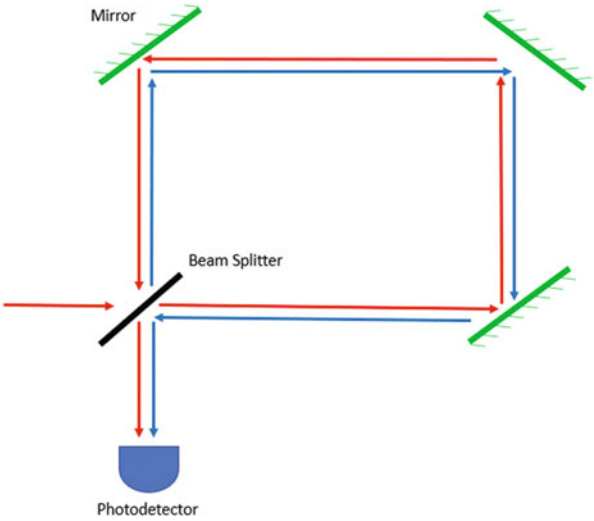

Fig. 8.6 Sagnac interferometer

8.2.6 Sagnac Interferometer

The Sagnac interferometer is based on the Sagnac effect. The phase difference between two counter propagating beams depends on the angular velocity of the rotating apparatus on which they are circulating.

Light is shined on the beam splitter that divides the wave into two counter propagating beams. They travel the same path on opposite directions and are then recombined on the exit point to interfere on the photodetector Fig. 8.6 (Kondrat et al. 2007).

The relation that links the rotating apparatus with the phase difference between the two beams is presented below:

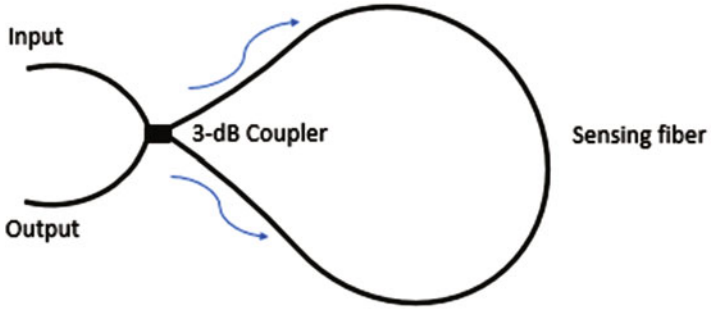

Fig. 8.7 Fiber-optic Sagnac interferometer

$$\Delta\varnothing = \frac{4\boldsymbol{A}\omega_{rot}}{\lambda v} \tag{8.3}$$

where, $\boldsymbol{A}$ is the unit vector perpendicular to the surface area of the apparatus; ω_{rot} is the angular velocity of the apparatus; λ is the light wavelength; and v is the beam speed.

Figure 8.7 shows the fiber optic version of the Sagnac Interferometer. The setup comprises an optical fiber loop and a 3-dB coupler. The latter splits the shined light into two beams that circulate the former in opposite directions. As long as the setup is stable, the phase difference of optical path between both waves is constant and zero. Introducing a rotation around the axis perpendicular to the figure plane the optical path difference (OPD) is determined by the polarization-dependent propagating velocity of the light mode guided along the path (Lee 2003).

8.2.7 Fabry–Pérot

The Fabry–Pérot (FP) sensor bases its working principle on the Fabry–Pérot interferometer (FPI). This type of optical system comprises two reflective parallel surfaces spaced apart at a certain distance from each other (Wei 2013). The shined light from a light source beams on the two parallel reflective surfaces under transmission and reflection rules. The interference occurs due to the continuous superposition of both the transmitted and reflected beams (Lee 2003).

FP sensors can be categorised into intrinsic and extrinsic (Tsai 2001). The former has reflecting components within the fiber itself by using optical elements, fiber defects, and chemical etching. The latter manipulates the reflection from an external cavity. In general, the cavity is in between the cleaved fiber and a membrane modulated depending on the external physical quantity to be monitored. The majority part of FP optical sensors is based on the same principle: they have an FP interferometer, whose cavity length changes according to the physical parameter

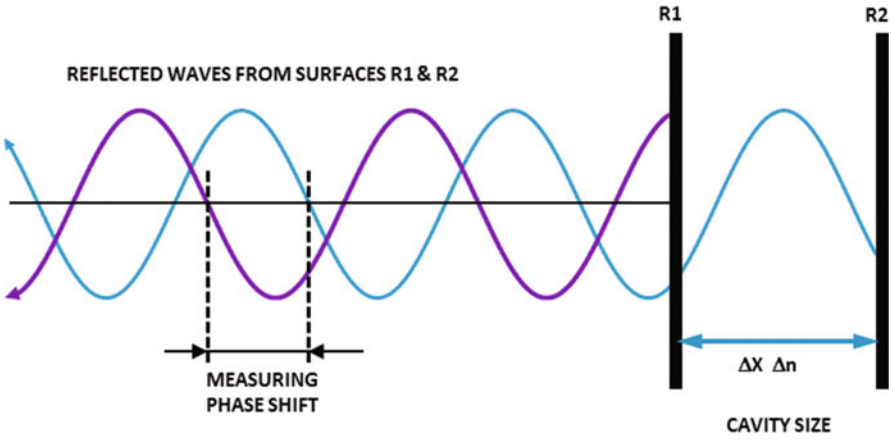

Fig. 8.8 Working principle of the FPI sensor, where ΔX is the change in length of the cavity and Δn is the change of the refractive index in the cavity

they are designed to measure. The cavity length is converted into the appropriate unit corresponding to the sensor type using appropriate sensor calibration (Pinet 2009).

The FP reflection (or transmission) spectrum is described as the wavelength-dependent intensity modulation of the input light source caused by the optical phase difference (wave imaginary part variation) between two reflected (or transmitted) beams. Constructive and destructive interference combines the maximum and minimum peaks in the 2π modulus. The phase difference is given as follows:

$$\Delta\varnothing_{FPI} = \frac{2\pi}{\lambda} n\, 2L \tag{8.4}$$

where, λ is the wavelength on the incident light; n is the refractive index of the cavity mode or cavity material; and L is the physical length of the cavity considering the light traveling back and forth (Rajan 2016).

Let us consider for instance a first fixed mirror and a second sensitive one (Fig. 8.8). Introducing an external perturbation to the sensor, the physical length of the cavity and/or the refractive index of the cavity material changes, producing a variation of the interferometer optical path difference (OPD). This affects the abovementioned phase difference. Applying a strain to the sensor, the cavity length and/or its optical property may change, thereby resulting in a phase variation.

8.2.8 Fiber Bragg Grating Sensors

FBG are the most common type of optical fiber sensors used in point strain or temperature measurement applications. FBG sensors are created by exposing the core of an optical fiber to a spatially modulated ultraviolet light pattern (Erdogan

1997). This exposed fiber length creates a refractive index modulation in the optical fiber core that partially reflects certain wavelengths of the input light to the fiber (Kersey et al. 1997). Different kinds of FBG sensors exhibit different behaviors based on how the refractive index modulation is realised. A few of the most common FBG types will be discussed in the next sections of this article, but in its most basic form, the grating period and the amplitude of the refractive index modulation are constant along the entire length of the FBG sensor. This is called a uniform FBG sensor, in which the peak wavelength of the reflected spectrum that is also called Bragg wavelength or λ_B linearly depends on the constant period (Λ) of the refractive index modulation and the effective refractive index of the fiber (n_{eff}) or

$$\lambda_B = 2\pi n_{\text{eff}} \Lambda. \tag{8.5}$$

From the above equation, the Bragg wavelength will shift toward higher wavelengths under tension and lower wavelengths under compression. The amount of strain or temperature change applied over the sensor length can be determined by tracking the shift of this peak wavelength of the reflection spectrum. In its simplified form, the relationship between the shift of the Bragg wavelength and the amount of strain or temperature change over the sensor length is presented as follows:

$$\Delta\lambda_{B_\epsilon} = k_s s \text{ and } \Delta\lambda_{B_T} = k_T \Delta T. \tag{8.6}$$

where s is the amount of strain change, k_s and k_T are constants determined by the optical fiber composition. For instance, in silica-based optical fibers operate at $\lambda_B = 1550$ nm, $k_s \approx 1.209 \times 10^{-3}$ nm/με, and $k_T = 10.075 \times 10^{-3}$ nm/°C (Kersey et al. 1997). Figure 8.9 depicts this linear behavior of FBG sensors under a uniform strain over its length.

The simplicity of the strain (or temperature) measurement algorithm, along with all the advantages of fiber optic sensing, has made FBG sensors an attractive alternative to electrical strain gauges and thermocouples.

8.2.9 Other FBG Grating Structures

If the grating period of the FBG has a uniform variation along its length, it will be called a linearly chirped FBG (LCFBG). Such chirped FBGs generally have a broader reflection spectrum and are mostly used as dispersive elements or filters in fiber optic communications (Xu et al. 1996), especially considering the fact that in ideal production conditions, they have a symmetrical reflection spectrum (Rajabzadeh 2018). However, they can also be used as sensors in strain or temperature demodulation, where instead of tracking the peak wavelength, the center of mass of the reflection spectrum is monitored (Erdogan 1997). Furthermore, they can be embedded within different composite structures for micro-crack detection

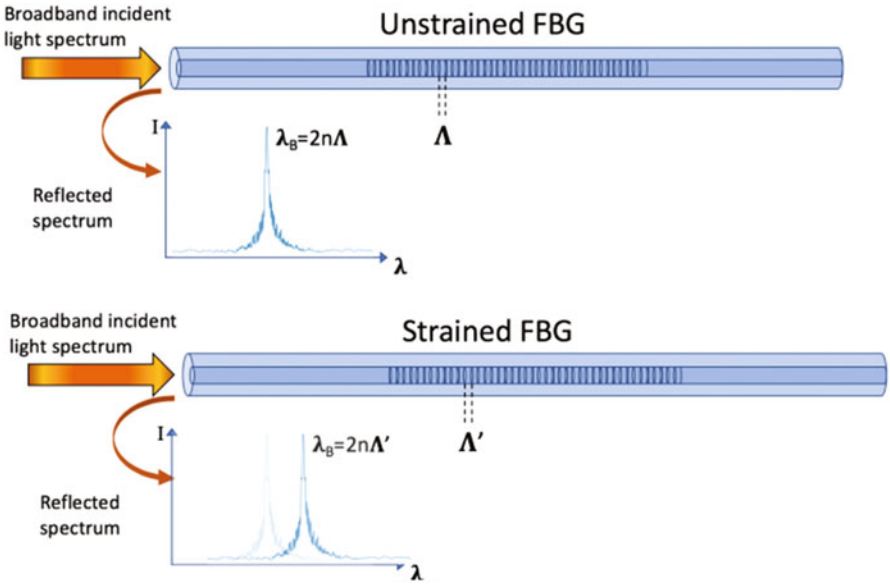

Fig. 8.9 Uniform FBG sensor under a uniform axial strain field

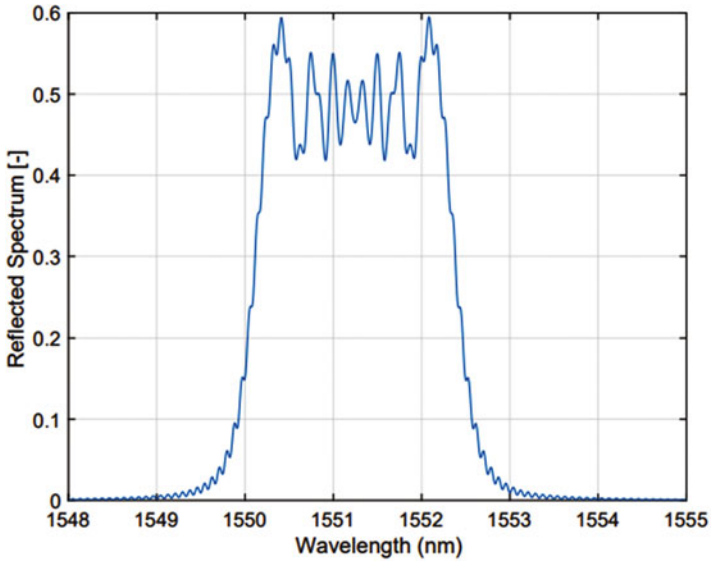

Fig. 8.10 Reflection spectrum from a linearly chirped FBG

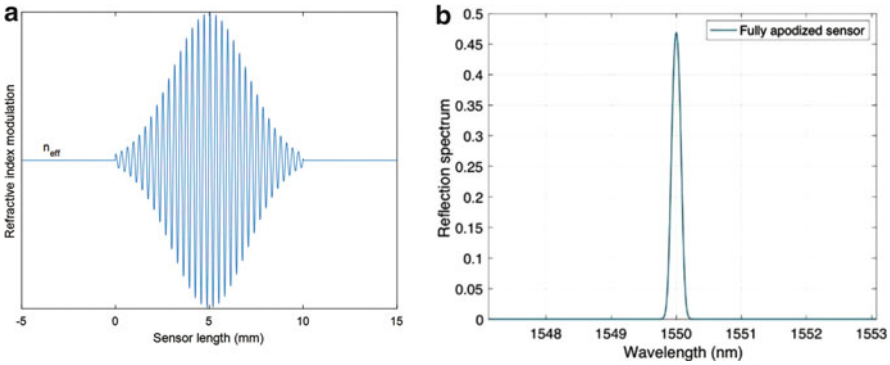

Fig. 8.11 (**a**) Gaussian apodization of the refractive index. (**b**) Apodised FBG sensor with fully suppressed side lobes

applications (Takeda et al. 2013). In Fig. 8.10 an example of the reflection spectrum of such a LCFBGs is given (with 10 mm length and a linear chirp rate of $\frac{d\lambda_B}{dz} = 2.5\ \mathrm{nm/cm}$).

In some FBG sensor applications, having side lobes in the reflection spectra is not ideal, and they must be suppressed as much as possible. A way of doing that is by apodizing the refractive index change along the sensor, which means the amplitude of the refractive index modulation follows a (Gaussian or raised cosine) pattern similar to that in Figure 8.11a. Figure 8.11b shows the suppressed side lobes of a Gaussian apodised FBG sensor.

Long-period gratings (LPGs) are another class of Bragg grating sensors, where the period of the grating is much larger than that of regular FBG sensors typically in the order of a few hundred nanometers to a few hundred micrometers (James and Tatam 2003). LPG sensors are mostly interesting for their transmission spectrum, where different attenuation bands correspond to different fiber cladding modes. These attenuation bands have different sensitivities to the different measurands applied over the sensor length, which allows them to be utilised for multi-parameter sensing elements capable of monitoring multiple environmental parameters independently.

Moreover, other kinds of FBG structures and types, such as tilted fiber Bragg gratings and phase-shifted FBGs, are also suitable for sensing a particular set of environmental parameters.

8.2.10 State-of-the Art Damage Detection Systems

In this paragraph three interrogators examples are reported. They make use of the optical interferometric principles and the readout techniques reported above in this chapter.

Fig. 8.12 DeltaSens interrogator by Optics11

DeltaSens: Fabry Perot Interrogator
The DeltaSens interrogator from Optics11 is a high-speed interrogation unit for reading Fabry–Pérot-type sensors. Optical sensors have to be properly coupled with DeltaSens, which will then communicate the sensed physical quantities to a computer to allow data processing. The readout must be equipped with the optical interface to manipulate and interpret the light.

DeltaSens (Fig. 8.12) interrogates multiple Fabry–Pérot-type sensors in an optical fiber network connected through standard optical splitters. The interferometer is formed by a broadband light source and a spectrometer. A spectral acquisition arrangement acquires successive spectral responses from the optical sensor arrangement during successive time intervals. All connected FP cavities with different cavity lengths result in specific footprints on the spectrometer. The spectral analysis arrangement detects a phase evolution of the periodicity throughout the successive spectral responses. The phase evolution of the periodicity provides a relatively precise measurement of a variation in an optical path length between the two reflective surfaces of the Fabry–Pérot structure. A variation in a physical quantity can cause optical path length variation. Accordingly, a relatively precise measurement of the physical quantity can be achieved (Grzegorz Gruca 2019).

The main application of such an interrogator is acceleration sensing using 1D and 3D optical accelerometers. The distances between each sensor and to the read-out can be kilometers (Rijnveld 2017). Further algorithms have been implemented to retrieve both the relative variation and the absolute value of the acceleration.

I4 Series: FBG Interrogators
Several methods can be used to interrogate FBG sensors, and a few of the most common techniques will be discussed herein. The most straightforward approach is to use a superluminescent diode (SLD) as a light source and a spectrometer to record the FBG-reflected spectrum (Alves 2003). However, the wavelength resolution and the accuracy offered by such spectrometers are usually above a few hundreds of picometers to a few nanometers, greatly limiting the strain and temperature resolution of the FBG sensor. Another approach is to use the fiber Fabry–Pérot tunable

Fig. 8.13 FAZT I4G interrogator

filter technology for a high-spatial resolution interrogation of the reflected spectrum. In this technique, a tunable laser and a high-precision synchronization system are used to scan the wavelength region of interest and sample the FBG-reflected spectrum (Ushakov 2015).

A similar alternative method is the interrogation of FBG sensors with the semiconductor tunable laser technology used in FAZ interrogators. This technology offers a sub-picometer wavelength accuracy that translates into micro-strain accuracy for strain measurements and temperature measurement accuracy of below 0.1 °C or ±1 με at scanning frequencies between 1 and 8 kHz (Fig. 8.13).

The I4 series can sustain up to 30 sensing points per channel. Different channel versions are produced: 4 and 16 with a trade-off between the number of sensing points and the sampling frequency.

8.2.11 Acoustic Emission Interrogator (OptimAE)

Acoustic emission (AE) is a non-invasive technique that allows the detection of damage and crack formation in engineering structures in real time (see Chap. 7). As a crack forms in such structures, the energy release results in transient surface acoustic waves, which are also called Rayleigh waves, that propagate throughout the material (Park 2011). Electrical AE systems use piezo-electric sensors to acquire these high-frequency acoustic waves. However, piezo-electric sensors have some limitations that narrow down their application in harsh environments.

The OptimAE unit is the optical acoustic emission monitoring system (Fig. 8.14). The optical AE setup contains two optical fibers (i.e., one operating as a sensing arm and one as a reference arm), which together form an interferometry setup. The sensing fiber is densely coiled on a metallic mandrel and is in a direct contact with the material surface for the optimum transmission of the surface acoustic wave to the sensor. The elastic energy of the acoustic wave stretches the fiber that changes the

Fig. 8.14 OptimAE acoustic emission monitoring system

differential length of the fibers on the sensing and the reference arms of the interferometer. The resulting interferometric signal is transferred to the OptimAE readout for signal acquisition, demodulation, and communication to the computer. The optical AE sensors can be sampled at 1 MS/s and have a spectral noise density of $150\, f\epsilon/\sqrt{Hz}$ (this term is the average amount of displacement noise per frequency bin which can be derived from power spectral analysis of the noise floor of the sensor response). They operate at a C-band wavelength range.

Performance tests showed that the optical acoustic emission sensors are a comparable alternative with respect to existing piezoelectric ones, opening new measurement scenarios in harsh environment conditions and extending the benefits of AE testing to new industries (Mario Sorgente 2020).

8.2.12 OFS Applications in Aeronautics

The optical fiber sensor technology and fiber Bragg gratings are evaluated as good tools for load monitoring and damage detection of aircraft structures (Guo et al. 2011; Mendoza et al. 2013) see overview in (Fig. 8.15). Di Sante gave a relatively recent overview of the major potential of OFS in the aeronautics industry (Di Sante 2015). Real-life OFS measurement campaigns on complete aircraft have been performed in the literature. A real-time analysis of wing deformations with a millimeter resolution allowed load interpretation during flight manoeuvres (Wada et al. 2019). Other researchers demonstrated the use of 780 FBG sensors to obtain out-of-plane loads and the wing deformations at various load levels (Nicolas, Sullivan and Richards 2016). OFS have also been used for wing shape deflection measurements of an ultralight carbon-composite aerial vehicle (Ma and Chen 2019).

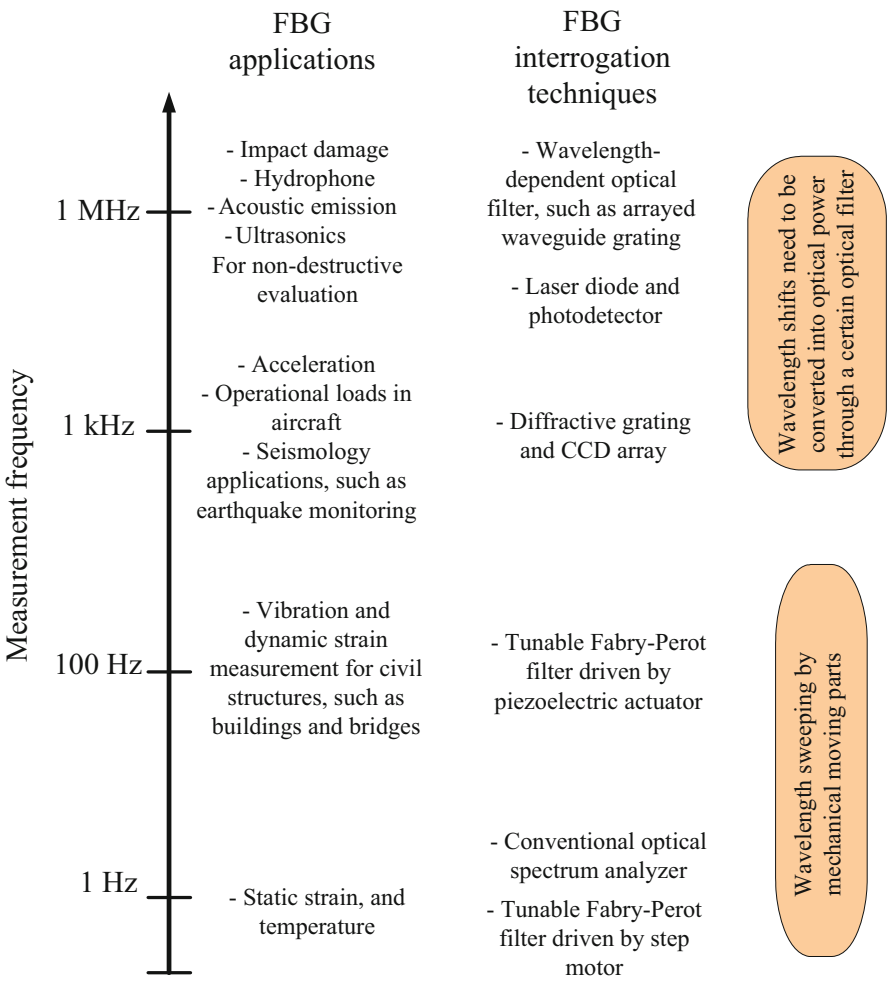

Fig. 8.15 Classification of FBG sensing techniques according to the frequency range (Guo et al. 2011)

Different types of embedded sensing solutions for the structural health monitoring of a helicopter blade, including FBG sensors and phased and discrete piezoelectric sensor arrays have been reported by Ghoshal et al. (2015). In addition to the potential use of OFS during operations and monitoring, these sensors also allow the production monitoring of aircraft components made from composite materials (Chiesura et al. 2016).

In addition to the vast opportunities in shell-type structures (wings, fuselage, etc.), OFS can also be used on solid components. García et al. (2015) used an intensity-modulated optical fiber sensor for tip clearance and tip timing measurements. Fiber sensors also enable load monitoring in landing gears (Iele et al. 2019).

Limitations and Challenges of Optical Fiber Sensors
Notwithstanding their immense application potential, optical fiber sensors also face some limitations, as is the case with any sensor type. Fiber integration is challenging, and care should be taken that debonding of the host composite material does not happen during the integration (Wang et al. 2012). Other researchers proposed the integration of a standard connector in the material (Sjögren 2000; Green and Shafir 1999). This facilitates the test process, but has an additional effect on the component strength (Sjögren 2001).

Another aspect related to the sensor integration is the fact that the optical response of the sensor might change after the embedding process (Luyckx et al. 2011). This generally does not pose any problem for the OFS operation, but in some situations like when the integration is poorly done, peak-splitting can occur. This peak-splitting can also occur because of a non-uniform loading (Kuang et al. 2001). In other words, a single Bragg peak will split in two separate peaks. In that case, ~~the~~ adapted signal processing algorithms should be used to consider the deformed state of the peak (Lamberti et al. 2014).

After integration in the material, the sensor is protected and can withstand high loads and temperatures. High-percentage strains can be reached in the case of polymer fiber (Zhou and Sim 2002; Peters 2011). However, the weakest point in the sensor system is the ingress or egress point where the fiber leaves the material. At this location, care should be taken not to apply high loads. In practice, a stress-relieve cover is often used to protect the fiber at the ingress/egress point. Accordingly, Missinne et al. (2017) proposed a special type of connector to detect a potential signal loss between the fiber and the connector.

Optical fiber sensors can be used to measure a variety of measurands (e.g., strain, pressure, temperature, etc.). However, it is not generally easy to separate these quantities if they appear simultaneously. One possible technique for simultaneously measuring strain and temperature is using so-called micro-structured optical fibers (Sonnenfeld et al. 2011).

8.3 Strain-Based SHM

Note that measuring strains is not the same as detecting damage. A local crack in a structure may significantly drop the failure loads, but until it grows toward the catastrophic failure, it produces negligible changes in most of the structure parameters (natural frequencies, global strain fields, etc.). The main difficulty for the SHM is identifying the 'features' or parameters sensitive to minor damages and distinguishing the response from natural and environmental disturbances.

If a crack does not change the strain field at the sensor location, it would not be detected, and the strain changes are quite small a few millimeters away from the crack tip, providing difficulties for a global SHM system based on strain monitoring. Figure 8.16 illustrates a few existing approaches:

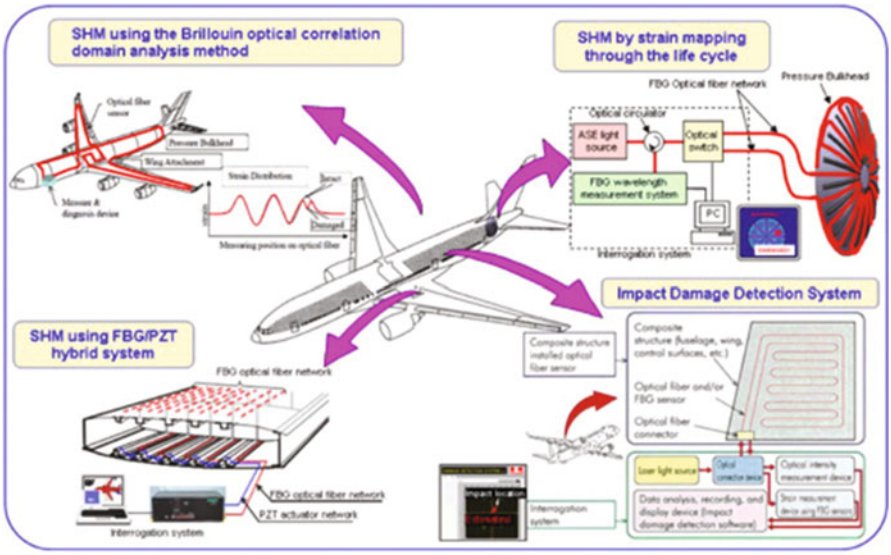

Fig. 8.16 Strain-based SHM systems in the METI Project (Takeda et al. 2013)

(a) Impact damage detection systems: by using FBGs as a high-frequency sensor for elastic waves, the impact location and its energy can be estimated similar to PZTs. Two main issues are the need of a wide structure coverage requiring a large number of sensors and the high sensitivity required in the interrogation system.
(b) Hybrid PZT–FBG sensors: similar to the former one, the elastic waves are produced by PZTs and detected by FBGs. Algorithms quite similar to those used for ultrasonics techniques are used.
(c) SHM by strain mapping: when the strains are measured at a very large number of points distributed throughout the structure and with adequate pattern recognition algorithms, the slight changes caused by a damage can be identified, even when the damage is not coincident with the sensor position. This is currently the most promising approach, even if the resolution is still not good enough (Sierra-Perez et al. 2013).
(d) SHM by distributed sensing: This is a procedure limited to optical fiber methods (either Brillouin or Rayleigh). When the optical fiber crosses a crack, this crack produces a local strain peak. Edge delamination in composite structures has been detected by this method (Güemes et al. 2018).

References

Alves JA (2003) Fiber Bragg sensor interrogation system based on a CCD spectrometer. Sensors:909–913

Anon. (1984) Strain gage instrumentation installed on the interior of the AFTI/F-16 wing NASA/Dryden Flight Research Center (NASA-DFRC) (p 1/1/1984)

ASTM E1561-93 (2014) Standard practice for analysis of strain gage rosette data. ASTM International, West Conshohocken, PA

ASTM E837-13a (2013) Standard test method for determining residual stresses by the hole-drilling strain-gage method. ASTM International, West Conshohocken, PA

Bahrampour AR (2012) Optical fiber interferometers and theirs application. Interferometry Res Appl Sci Technol. https://doi.org/10.5772/34346

Chiesura G, Lamberti A, Yang Y et al (2016) RTM production monitoring of the A380 hinge arm droop nose mechanism: a multi-sensor approach. Sensors 16. https://doi.org/10.3390/s16060866.

Cranch GA, Nash PJ (2001) Large-scale multiplexing of interferometric fiber-optic sensors using TDM and DWDM. J Lightwave Technol 19:687–699. https://doi.org/10.1109/50.923482

Dai Y, Liu Y, Leng J et al (2009) A novel time-division multiplexing fiber Bragg grating sensor interrogator for structural health monitoring. Opt Lasers Eng 47:1028–1033. https://doi.org/10.1016/j.optlaseng.2009.05.012

Dawood TA, Shenoi RA, Sahin M (2007) A procedure to embed fibre Bragg grating strain sensors into GFRP sandwich structures. Compos A 38:217–226. https://doi.org/10.1016/j.compositesa.2006.01.028

Di Sante R (2015) Fibre optic sensors for structural health monitoring of aircraft composite structures: recent advances and applications. Sensors (Switzerland) 15:18666–18713. https://doi.org/10.3390/s150818666

Druet T, Chapuis B, Jules M et al (2018) Passive guided waves measurements using fiber Bragg gratings sensors. J Acoust Soc Am 144:1198. https://doi.org/10.1121/1.5054015.

Erdogan T (1997) Fiber grating spectra. J Lightwave Technol 15:1277–1294. https://doi.org/10.1109/50.618322

Faisal NH et al (2019) Diametral compression test method to analyse relative surface stresses in thermally sprayed coated and uncoated circular disc specimens. Surface Coatings Technol 357:497–514

Froggatt M et al (1998) High-spatial-resolution distributed strain measurement in optical fiber with Rayleigh scatter. Appl Opt 37(10):1735–1740

García I, Zubia J, Durana G et al (2015) Optical fiber sensors for aircraft structural health monitoring. Sensors (Switzerland) 15:15494–15519. https://doi.org/10.3390/s150715494

Garus D, Krebber K, Schliep F et al (1996) Distributed sensing technique based on Brillouin optical-fiber frequency-domain analysis. Opt Lett 21(/17):1402–1404. https://doi.org/10.1364/OL.21.001402

Ghoshal A, Ayers J, Gurvich M et al (2015) Experimental investigations in embedded sensing of composite components in aerospace vehicles. Compos Part B Eng 71:52–62. https://doi.org/10.1016/j.compositesb.2014.10.050

Giraldo CM, Sagredo JZ, Gómez JS et al (2017) Demonstration and methodology of structural monitoring of stringer runs out composite areas by embedded optical fiber sensors and connectors integrated during production in a composite plant. Sensors (Basel, Switzerland) 17. https://doi.org/10.3390/s17071683.

Girard S et al (2018) Recent advances in radiation-hardened fiber-based technologies for space applications. J Opt (United Kingdom) 9:20. https://doi.org/10.1088/2040-8986/aad271

Goossens S, De Pauw B, Geernaert T et al (2019) Aerospace-grade surface mounted optical fibre strain sensor for structural health monitoring on composite structures evaluated against in-flight conditions. Smart Mater Struct 28. https://doi.org/10.1088/1361-665X/ab1458

Grandal T, Zornoza A, Fraga S et al (2018) Laser cladding-based metallic embedding technique for fiber optic sensors. J Lightwave Technol 36:1018–1025. https://doi.org/10.1109/JLT.2017.2748962.

Green AK, Shafir E (1999) Termination and connection methods for optical fibres embedded in aerospace composite components. Smart Mater Struct 8:269–273. https://doi.org/10.1088/0964-1726/8/2/013

Grzegorz Gruca NR (2019). United States Patent No. US, 10, p 255 B2

Güemes A, Fernández-López A, Díaz-Maroto PF et al (2018) Structural health monitoring in composite structures by fiber-optic sensors. Sensors 18:1094. https://doi.org/10.3390/s18041094

Guo H, Xiao G, Mrad N et al (2011) Fiber optic sensors for structural health monitoring of air platforms. Sensors 11:3687–3705. https://doi.org/10.3390/s110403687.

Hariharan P (2007) Basics of interferometry, Academic Presse, ISBN: 978-0-12-373589-8, https://doi.org/10.1016/B978-0-12-373589-8.X5000-7.

Havermann D, Mathew J, MacPherson WN et al (2015) Temperature and strain measurements with fiber Bragg gratings embedded in stainless steel 316. J Lightwave Technol 33:2474–2479. https://doi.org/10.1109/JLT.2014.2366835.

He XL, Wang ZQ, Wang DH et al (2019) Optical fiber sensor for strain monitoring of metallic device produced by very high-power ultrasonic additive Manufacturing. IEEE Sensors J IEEE 19:10680–10685. https://doi.org/10.1109/JSEN.2019.2928966.

Iele A et al (2019) A fiber optic sensors system for load monitoring on aircraft landing Gears. In: Kalli K, Brambilla G, OKeeffe S (eds) Opt Eng (proc SPIE) seventh European workshop on optical fibre sensors (EWOFS 2019). SPIE-International Society, Bellingham, WA, pp 98227–90010. https://doi.org/10.1117/12.2541110.

IPC/JEDEC (2005) Printed wiring board strain gage test guideline JEDEC. IPC/JEDEC-9704

James SW, Tatam RP (2003) Optical fibre long-period grating sensors: characteristics and application. Meas Sci Technol 14:R49–R61. https://doi.org/10.1088/0957-0233/14/5/201

Kersey AD, Davis MA, Patrick HJ et al (1997) Fiber grating sensors. J Lightwave Technol 151442-1463. https://doi.org/10.1109/50.618377.

Kinet D, Mégret P, Goossen KW et al (2014) Fiber Bragg grating sensors toward structural health monitoring in composite materials: challenges and solutions. Sensors (Switzerland) 14:7394–7419. https://doi.org/10.3390/s140407394

Kondrat M et al (2007) A Sagnac-Michelson fibre optic interferometer: signal processing for disturbance localization. Opto-Electronics Review 15:127–132

Kuang KSC, Kenny R, Whelan MP et al (2001) Embedded fibre Bragg grating sensors in advanced composite materials. Compos Sci Technol 61:1379–1387. https://doi.org/10.1016/S0266-3538(01)00037-9.

Lamberti A, Vanlanduit S, De Pauw B et al (2014) A novel fast phase correlation algorithm for peak wavelength detection of fiber Bragg grating sensors. Opt Express 22:7099–7112. https://doi.org/10.1364/OE.22.007099.

Lee B (2003) Review of the present status of optical fiber sensors. Opt Fiber Technol 9:57–79. https://doi.org/10.1016/S1068-5200(02)00527-8

Loutas TH, Charlaftis P, Airoldi A et al (2015) Reliability of strain monitoring of composite structures via the use of optical fiber ribbon tapes for structural health monitoring purposes. Compos Struct 134:762–771. https://doi.org/10.1016/j.compstruct.2015.08.100

Luyckx G, Voet E, Lammens N et al (2011) Strain measurements of composite laminates with embedded fibre Bragg gratings: criticism and opportunities for research. Sensors 11:384–408. https://doi.org/10.3390/s110100384.

Ma Z, Chen X (2019) Fiber Bragg gratings sensors for aircraft wing shape measurement: recent applications and technical analysis. Sensors (Switzerland) 19. https://doi.org/10.3390/s19010055

Malik SA, Wang L, Curtis PT et al (2016) Self-sensing composites: in-situ detection of fibre fracture. Sensors (Switzerland) 16:1–18. https://doi.org/10.3390/s16050615

Mario Sorgente AR (2020) Performance comparison between fiber-optic and piezoelectric acoustic emission sensors.

Mendoza E et al (2013) In-flight fiber optic acoustic emission sensor (FAESense) system for the real time detection, localization, and classification of damage in composite aircraft structures. Photon Appl Aerosp Comm Harsh Environ IV 8720:87200K. https://doi.org/10.1117/12.2018155

Mihailov SJ (2012) Fiber Bragg grating sensors for harsh environments. Sensors 12:1898–1918. https://doi.org/10.3390/s120201898

Missinne J, Luyckx G, Voet E et al (2017) Low-loss connection of embedded optical fiber sensors using a self-written waveguide. IEEE Photon Technol Lett 29:1731–1734. https://doi.org/10.1109/LPT.2017.2747630.

Nedjalkov A, Meyer J, Waltermann C et al (2018) Direct inscription and evaluation of fiber Bragg gratings in carbon-coated optical sensor glass fibers for harsh environment oil and gas applications. Appl Opt 57:7515–7525. https://doi.org/10.1364/AO.57.007515.

Nicolas MJ, Sullivan RW, Richards WL (2016) Large scale applications using FBG sensors: determination of in-flight loads and shape of a composite aircraft wing. Aerospace 3. https://doi.org/10.3390/aerospace3030018

Park S-JA-K (2011) Interface science and composites. Academic Press, Cambridge, MA

Peters K (2011) Polymer optical fiber sensors - a review. Smart Mater Struct 20. https://doi.org/10.1088/0964-1726/20/1/013002

Pinet É (2009) Fabry-Pérot fiber-optic sensors for physical parameters. J Sens 2009:1–9. https://doi.org/10.1155/2009/720980

Rajabzadeh AA (2018) Analysis of FBG reflection spectra under anti-symmetrical strain distributions using the approximated transfer matrix model Optical sensing and detection V (p. 106800O). International Society for Optics and Photonics, Strasbourg

Rajan G (2016) Structural health monitoring of composite structures using fiber optic methods. CRC Press, Boca Raton

Rijnveld N (2017) Optical fibre interferometry – new concepts and applications. Mikroniek 18–21

Saheb N, Mekid S (2015) Fiber-embedded metallic materials: from sensing towards nervous behavior. Materials 8:7938–7961. https://doi.org/10.3390/ma8115435

Sjögren A (2000) Manufacturing technique for embedding detachable fiber-optic connections in aircraft composite components. Smart Mater Struct 9:855–858. https://doi.org/10.1088/0964-1726/9/6/316

Sjögren BA (2001) Static strength of CFRP laminates with embedded fiber-optic edge connectors. Compos A 32:189–196. https://doi.org/10.1016/S1359-835X(00)00138-X

Sonnenfeld C, Sulejmani S, Geernaert T et al (2011) Microstructured optical fiber sensors embedded in a laminate composite for smart material applications. Sensors 11:2566–2579. https://doi.org/10.3390/s110302566.

Takeda NA et al (2013) Outline of the Japanese National Project on Structural Health Monitoring System for Aircraft Composite Structures and JASTAC Project. IWSHM2013, Stanford

Takeda NA (2005) Development of smart composite structures with small-diameter fiber Bragg grating sensors for damage detection: quantitative evaluation of delamination length in CFRP laminates using lamb wave sensing. Compos Sci Technol 2005:2575–2587

Takeuchi K (2012) Locations of strain gauges for fatigue analysis of welded joints (2). Weld Int 26:655–664. https://doi.org/10.1080/09507116.2011.590680

Tsai W (2001) A novel structure for the intrinsic Fabry-Perot fiber-optic temperature sensor. J Lightw Techol

Ushakov NA (2015) Utilization of NI PXIe-4844 interrogator for high resolution fiber extrinsic Fabry-Perot interferometric sensing. In: 2015 International Siberian conference on control and communications (SIBCON). IEEE, pp 1–4

Wada D, Igawa H, Tamayama M et al (2019) Flight demonstration of aircraft wing monitoring using optical fiber distributed sensing system. Smart Mater Struct 28. https://doi.org/10.1088/1361-665X/aae411

Wang Y, Gong J, Dong B et al (2012) A large serial time-division multiplexed Fiber Bragg grating sensor network. J Lightwave Technol IEEE 30:2751–2756. https://doi.org/10.1109/JLT.2012.2205897.

Wei US (2013) Fiber optic interferometric devices. Springer Science, Cham

Xu MG, Alavie AT, Maaskant R et al (1996) Tunable fibre bandpass filter based on a linearly chirped fibre Bragg grating for wavelength demultiplexing. Electron Lett 32:1918–1919. https://doi.org/10.1049/el:19961242

Yu F, Okabe Y (2017) Fiber-optic sensor-based remote acoustic emission measurement in a 1000 °C environment. Sensors (Switzerland) 17. https://doi.org/10.3390/s17122908

Zahid MN et al (2019) Reflectometric and interferometric fiber optic sensor's principles and applications. Springer, Cham

Zetie KP, Adams SF, Tocknell RM (2000) How does a Mach-Zehnder interferometer work? Westminster School Phys Educ 35:46–48. https://doi.org/10.1088/0031-9120/35/1/308

Zhou G, Sim LM (2002) Damage detection and assessment in fibre-reinforced composite structures with embedded fibre optic sensors-review. Smart Mater Struct 11:925–939. https://doi.org/10.1088/0964-1726/11/6/314